Reminder: Magnetic structures description and determination by neutron diffraction

E. Ressouche

Collection SFN **13**, 02001 (2014)
DOI: 10.1051/sfn/20141302001

Reminder: Magnetic structures description and determination by neutron diffraction

E. Ressouche

SPSMS, UMR-E CEA/UJF-Grenoble 1, INAC, 38054 Grenoble, France

Abstract. The most widespread use of neutron diffraction is of course the determination of magnetic structures, that is the determination of the directions in which moments point in a magnetically ordered material. To describe magnetic structures, it is intuitive and convenient to relate them to the underlying crystal structures, and therefore to use unit cells. But such a simplification misses the elegance of what magnetic structures really are and even makes their description more complex, or impossible in some cases. A more general formalism is required, the formalism of propagation vectors. This lecture is a reminder on what this formalism is, how it can describe the more general structures and how it enters fundamental equations at the basis of magnetic structure determinations by neutron diffraction.

1. INTRODUCTION

The power of neutron scattering relies mainly on the unique physical properties of this particle. Its mass gives to the neutron, once thermalized, a de Broglie wavelength comparable to interatomic distances in crystals ($1 - 3$ Å), allowing an interference effect when scattered from condensed matter systems. This interference effect is used to determine both the nuclear structures and the magnetic ones. An even more important consequence of the mass is the energy of thermal neutrons (10–80 meV), energy particularly well suited to study both nuclear and magnetic thermal excitations. Because of its electrical neutrality, the neutron possesses a huge penetrating power, and therefore is able to probe the complete volume of a sample and not only a small region near the surface. In addition, from the experimental point of view, this property allows to use bulky and sophisticated pieces of equipment such as cryostats, dilution refrigerators, high-field cryomagnets and/or pressure cells. Last but not least, the nuclear spin of the neutron undergoes a dipole-dipole interaction with the unpaired electrons in a magnetic material. This interaction is comparable in strength to the interaction with the nuclei, so that magnetic properties can be investigated at a microscopic scale with a high precision.

Detailed accounts of the theory of neutron scattering have been given in many textbooks [1–5], and is repeated in the lecture of M. Enderle in this one: it is not the aim of this section to reproduce them. Only some of the fundamental ideas, intended to be complete enough to cover our needs, are presented in what follows.

2. ELASTIC NEUTRON SCATTERING

The elastic scattering by a target of an incident beam of neutrons characterized by a wave vector $\boldsymbol{k}_i$ and a spin σ_i ($\boldsymbol{\sigma}$ is the Pauli spin matrix) into a final state characterized by $\boldsymbol{k}_f$ and σ_f, is given, within the Born approximation, by the differential cross-section:

$$\frac{d\sigma}{d\Omega}(\boldsymbol{k}_f\sigma_f, \boldsymbol{k}_i\sigma_i) = \left(\frac{m}{2\pi\hbar^2}\right)^2 \left| <\boldsymbol{k}_f\sigma_f|V(\boldsymbol{r})|\boldsymbol{k}_i\sigma_i> \right|^2 \tag{2.1}$$

where $V(\boldsymbol{r})$ is the potential felt by a neutron at $\boldsymbol{r}$ in the field of the scatterer and m its mass. A useful concept is that of the scattering amplitude operator $a(\boldsymbol{Q})$. Assuming $|\boldsymbol{k}_i| = |\boldsymbol{k}_f|$, (elastic scattering) and $\boldsymbol{Q} = \boldsymbol{k}_i - \boldsymbol{k}_f$ being the scattering vector, one can write:

$$\left(\frac{m}{2\pi\hbar^2}\right) <\boldsymbol{k}_f\sigma_f|V(\boldsymbol{r})|\boldsymbol{k}_i\sigma_i> = <\sigma_f|a(\boldsymbol{Q})|\sigma_i> \tag{2.2}$$

Eq. (2.1) thus becomes:

$$\frac{d\sigma}{d\Omega}(\boldsymbol{k}_f\sigma_f, \boldsymbol{k}_i\sigma_i) = \left| <\sigma_f|a(\boldsymbol{Q})|\sigma_i> \right|^2 . \tag{2.3}$$

2.1 Nuclear scattering amplitude from bound nuclei

Because the nucleon-nucleon interaction has a very short range which is much less than the wavelength of thermal neutrons, the nuclear scattering is isotropic and can therefore be characterized by a single parameter b_i, called the scattering length. The potential takes the form:

$$V_N(\boldsymbol{r}) = \frac{2\pi\hbar^2}{m}\, b_i\, \delta(\boldsymbol{r} - \boldsymbol{R}) \tag{2.4}$$

where $\boldsymbol{R}$ denotes the position of the nucleus. This scattering length is different not only for each atom but also for each isotope. Moreover, it depends on the relative coupling between the neutron spin and the nuclear spin I of the isotope. When the temperature is high enough for the nuclear polarization to be negligible ($T >$ a few tenths of a Kelvin), this dependency can be omitted, and the nuclear scattering amplitude for a single isotope nucleus is simply:

$$a_N(\boldsymbol{Q}) = b_i. \tag{2.5}$$

In turn, the differential cross section for the coherent scattering of an unpolarized neutron beam by a natural nucleus without nuclear polarization becomes:

$$\left(\frac{d\sigma_N}{d\Omega}\right) = |\bar{b}|^2 \tag{2.6}$$

the average being taken over the isotope populations of the natural element (defining a so called average nucleus). Actually, it exists another contribution, due to the distribution of the isotopes, which reflects the random deviations of the scattering lengths from the mean value $\bar{b}$. This term does not contribute at all to the coherent scattering in a crystal and leads to incoherent scattering.

2.2 Magnetic scattering amplitude

The magnetic interaction is due to the coupling of the neutron spin with the magnetic field $\boldsymbol{H}$ arising from unpaired electrons. If the field is due to N unpaired electrons i whose positions are $\boldsymbol{R}_i$, the potential

of a neutron at $\boldsymbol{r}$ takes the form:

$$V_M(\boldsymbol{r}) = -\boldsymbol{\mu}_n \cdot \boldsymbol{H}(\boldsymbol{r}) = -\boldsymbol{\mu}_n \sum_{i=1}^{N} \left(curl \left(\frac{\boldsymbol{\mu}_i \times (\boldsymbol{r} - \boldsymbol{R}_i)}{|\boldsymbol{r} - \boldsymbol{R}_i|^3} \right) - \frac{2\mu_B \, \boldsymbol{p}_i \times (\boldsymbol{r} - \boldsymbol{R}_i)}{\hbar \, |\boldsymbol{r} - \boldsymbol{R}_i|^3} \right) \tag{2.7}$$

where $\boldsymbol{\mu}_n = \gamma \mu_N \boldsymbol{\sigma}$ is the neutron moment (μ_N and γ (negative) being respectively the nuclear Bohr magneton and the gyromagnetic ratio) and $\boldsymbol{\mu}_i = -2\mu_B \boldsymbol{s}_i$, $\boldsymbol{s}_i$ is the spin of the unpaired electron i and $\boldsymbol{p}_i$ its momentum. This potential has two contributions, the first one being the classical dipolar interaction due to the spin of electrons whereas the second term arises from the orbital motion. Replacing this potential in Eq. (2.2) allows to define a magnetic scattering amplitude operator which can be written as:

$$a_M(\boldsymbol{Q}) = p \, \boldsymbol{\sigma} \cdot [\hat{Q} \times \mathcal{M}(\boldsymbol{Q}) \times \hat{Q}]. \tag{2.8}$$

In this expression $\mathcal{M}(\boldsymbol{Q})$ is the Fourier transform of the **total magnetization density** $\mathcal{M}(\boldsymbol{r})$, with both spin and orbital contributions:

$$\mathcal{M}(\boldsymbol{r}) = \mathcal{M}_S(\boldsymbol{r}) + \mathcal{M}_L(\boldsymbol{r}) \tag{2.9}$$

$p = (m/2\pi\hbar^2)4\pi\gamma\mu_N\mu_B = 0.2696 \times 10^{-12}$ cm is a constant which represents the scattering amplitude at $Q = 0$ for a 1 μ_B single magnetic moment, and $\hat{Q} = \boldsymbol{Q}/|\boldsymbol{Q}|$ is a unitary vector along $\boldsymbol{Q}$.

The expression of this magnetic scattering amplitude operator is more complex than its nuclear counterpart because the magnetic interaction is long range and noncentral. The term $\hat{Q} \times \mathcal{M}(\boldsymbol{Q}) \times \hat{Q}$ is the projection of $\mathcal{M}(\boldsymbol{Q})$, the Fourier transform of the magnetization density, in the plane perpendicular to the scattering vector and is often denoted as $\mathcal{M}_\perp(\boldsymbol{Q})$. This angular dependance of the scattering amplitude allows to determine both the amplitude and the direction of the magnetic moment. However, this form is not very useful to handle magnetic structure calculations, and one defines generally a so called magnetic form factor for each individual atom which allows to write:

$$a_M(\boldsymbol{Q}) = p \, f(Q) \, \boldsymbol{\mu}_\perp \cdot \boldsymbol{\sigma} \tag{2.10}$$

$f(Q)$ is the form factor of the magnetic ion, with $f(Q = 0) = 1$, $\boldsymbol{\mu}$ is the magnetic moment carried by the atom, $\boldsymbol{\mu}_\perp$ being its projection onto the plane perpendicular to the scattering vector.

The differential cross section for the magnetic scattering of an **unpolarized neutron beam** by such a magnetic ion is therefore:

$$\left(\frac{d\sigma_M}{d\Omega} \right) = p^2 f(Q)^2 \mu_\perp^2. \tag{2.11}$$

2.3 Scattering from a crystal

Let us consider a single crystal containing several atoms per unit cell. Such a crystal is called a non-Bravais crystal (by opposition, a Bravais crystal contains only one atom per unit cell). Let $\boldsymbol{R}_{n\nu}$ be the position of atom number ν in the cell number n[1]:

$$\boldsymbol{R}_{n\nu} = \boldsymbol{R}_n + \boldsymbol{r}_\nu \tag{2.12}$$

where $\boldsymbol{R}_n = n_a\boldsymbol{a} + n_b\boldsymbol{b} + n_c\boldsymbol{c}$ (n_a, n_b, n_c integers) is the position of cell number n compared to an arbitrary origin in the crystal, $\boldsymbol{r}_\nu = x_\nu\boldsymbol{a} + y_\nu\boldsymbol{b} + z_\nu\boldsymbol{c}$ (x_ν, y_ν, z_ν are the atomic positions defined in the International Tables) is the position of atom ν in this cell and $\boldsymbol{a}$, $\boldsymbol{b}$, $\boldsymbol{c}$ are the unit cell vectors.

[1] Actually the label ν should be splitted in two, since for most of the space groups, the unit cell contains several kind of atoms located in **different equivalent sites**. This notation with only one label means that between these ν atoms, some are related to each others by the symmetry operators of the crystallographic space group.

From the unit cell, one can define a reciprocal lattice by three vectors (V is the volume of the unit cell)[2]:

$$\begin{aligned} \boldsymbol{a}^* &= 2\pi \frac{\boldsymbol{b} \times \boldsymbol{c}}{V} \\ \boldsymbol{b}^* &= 2\pi \frac{\boldsymbol{c} \times \boldsymbol{a}}{V} \\ \boldsymbol{c}^* &= 2\pi \frac{\boldsymbol{a} \times \boldsymbol{b}}{V}. \end{aligned} \tag{2.13}$$

The volume of the reciprocal unit cell is $(2\pi)^3/V$. A reciprocal lattice vector is thus defined as $\boldsymbol{Q} = h\,\boldsymbol{a}^* + k\,\boldsymbol{b}^* + l\,\boldsymbol{c}^*$.

For an **unpolarized neutron beam**, there is no interference between the nuclear and the magnetic scattering, and the differential elastic cross section for such a crystal is:

$$\frac{d\sigma}{d\Omega}(\boldsymbol{Q}) = \frac{d\sigma_N}{d\Omega}(\boldsymbol{Q}) + \frac{d\sigma_M}{d\Omega}(\boldsymbol{Q}). \tag{2.14}$$

The nuclear interaction potential in the crystal is:

$$V_N(\boldsymbol{r}) = \frac{2\pi\hbar^2}{m} \sum_{n,\nu} b_\nu\, \delta(\boldsymbol{r} - \boldsymbol{R}_{n\nu}) \tag{2.15}$$

and

$$\begin{aligned} \frac{d\sigma_N}{d\Omega}(\boldsymbol{Q}) &= \left| < \boldsymbol{k}_f\, \boldsymbol{\sigma}_f | \sum_{n,\nu} b_\nu\, \delta(\boldsymbol{r} - \boldsymbol{R}_{n\nu}) | \boldsymbol{k}_i\, \boldsymbol{\sigma}_i > \right|^2 \\ &= \left| \sum_{n,\nu} b_\nu\, e^{i\,\boldsymbol{Q}\cdot\boldsymbol{R}_{n\nu}} \right|^2 \\ &= \frac{(2\pi)^3}{V}\, \mathcal{N} \sum_{\boldsymbol{H}} |F_N(\boldsymbol{Q})|^2\, \delta(\boldsymbol{Q} - \boldsymbol{H}) \end{aligned} \tag{2.16}$$

where $\mathcal{N}$ is the number of unit cells contained in the crystal. In this expression, $F_N(\boldsymbol{Q})$ is the **unit cell nuclear structure factor**, defined as[3]:

$$F_N(\boldsymbol{Q}) = \sum_\nu b_\nu\, e^{i\,\boldsymbol{Q}\cdot\boldsymbol{r}_\nu}. \tag{2.17}$$

The sum $\sum_\nu$ is taken over the atoms of the **unit cell**. The relation $\boldsymbol{Q} = \boldsymbol{H}$ arising from the δ function in Eq. (2.16) is nothing but the Bragg condition of reflection. It demonstrates that a coherent elastic scattering occurs in a perfect crystal only for scattering vectors that **coincide with a reciprocal lattice vector**. This result is purely a consequence of the symmetry of the crystal lattice and does not depend upon the nature of the neutron-lattice interaction. This last result, derived in the case of nuclear scattering, can be extended to the magnetic scattering. This generalization is presented in the next section.

---

[2] Note the difference of definition compared to the usual crystallographic convention where $\boldsymbol{a}^* = \boldsymbol{b} \times \boldsymbol{c}/V \ldots$

[3] To take into account thermal displacement around equilibrium positions, each term of the sum has to be multiplied by e^{-W_ν}, W_ν being the Debye-Waller factor of atom number ν.

3. MAGNETIC STRUCTURES AND PROPAGATION VECTORS

The main difficulty when dealing with magnetic structures arises from the fact that even if they are periodical, these structures do not have necessarily the same periodicity than the underlying crystallographic ones. Two different languages are used to describe them. The first one is well adapted to simple cases, in which the periodicity of the magnetic structure is equal or is an integral multiple of the nuclear one, and gives an image of the mutual orientations of the magnetic moments within the cells: structures are described in the usual terms of ferromagnetic, antiferromagnetic or ferrimagnetic main classes. The second language is more rigorous, better adapted both to complex structures and to neutron diffraction, and refers to the reciprocal space. This language describes the structures in terms of propagation vectors.

3.1 Definition of the propagation vectors

If we return to the single crystal we defined in the previous section, and if we assume now that all the atoms (n, ν) carry a magnetic moment, one can define a vector $\boldsymbol{\mu}_{n\nu}$ for each of these atoms giving the amplitude and the direction of this magnetic moment. In the ordered state, and whatever the nature of the ordering, this moment distribution, which is a periodic function of space, can be Fourier expanded according to:

$$\boldsymbol{\mu}_{n\nu} = \sum_{\boldsymbol{k}} \boldsymbol{m}_{\nu,\boldsymbol{k}}\, e^{-i\ \boldsymbol{k}\cdot\boldsymbol{R}_n} \tag{3.1}$$

where $\boldsymbol{m}_{\nu,\boldsymbol{k}}$ is the Fourier component of the distribution associated to the progation vector $\boldsymbol{k}$. Because the magnetic atoms have a **positional periodicity given by the underlying nuclear structure**, one can show that the wave vectors $\boldsymbol{k}$ that enter the summation are periodic in the reciprocal space and hence can be chosen within **the first Brillouin zone** of the Bravais lattice of the nuclear unit cell. In turn, the differential magnetic cross section can be written as:

$$\frac{d\sigma_M}{d\Omega}(\boldsymbol{Q}) = \frac{(2\pi)^3}{V}\ N \sum_{\boldsymbol{H}} \sum_{\boldsymbol{k}} |\boldsymbol{F}_{M\perp}(\boldsymbol{Q})|^2\, \delta(\boldsymbol{Q} - \boldsymbol{H} - \boldsymbol{k}) \tag{3.2}$$

where the **magnetic structure factor** $\boldsymbol{F}_M$ is defined as:

$$\boldsymbol{F}_M(\boldsymbol{Q} = \boldsymbol{H} + \boldsymbol{k}) = p \sum_{\nu} f_\nu(\boldsymbol{Q})\, \boldsymbol{m}_{\nu,\boldsymbol{k}}\, e^{i\ \boldsymbol{Q}\cdot\boldsymbol{r}_\nu} \tag{3.3}$$

$\boldsymbol{F}_{M\perp}$, often called the magnetic interaction vector and denoted $\mathbf{M}_\perp$ in the lecture on polarized neutron, is the projection of $\boldsymbol{F}_M$ in the plane perpendicular to $\boldsymbol{Q}$. The expression Eq. (3.2) of the differential magnetic cross section means that inside **each Brillouin zone of the nuclear unit cell** defined by the lattice vectors $\boldsymbol{H}$, it exists **as many superlattice magnetic peaks as there are distinct propagation vectors** $\boldsymbol{k}$ in the expansion Eq. (3.1). These peaks are located at **reciprocal points defined by the scattering vectors** $\boldsymbol{Q} = \boldsymbol{H} + \boldsymbol{k}$. In the expression Eq. (3.3) of the magnetic structure factor, the sum $\sum_\nu$ is taken over the atoms of the unit cell, as for the nuclear structure factor. An important consequence of the term $|\boldsymbol{F}_{M\perp}(\boldsymbol{Q})|^2$ is that, when all the vectors $\boldsymbol{m}_{\nu,\boldsymbol{k}}$ are collinear and parallel to the scattering vector $\boldsymbol{Q}$, the differential cross section, and therefore the intensity of this magnetic peak, is zero.

Before going further, two remarks are necessary:

- the magnetic structure factor $\boldsymbol{F}_M$ is a **vector** which may be either real, purely imaginary or complex in the general case, whereas the nuclear structure factor F_N is a **scalar** (which also may be complex).
- in Eq. (3.1), both $e^{-i\ \boldsymbol{k}\cdot\boldsymbol{R}_n}$ and $\boldsymbol{m}_{\nu,\boldsymbol{k}}$ are **complex quantities** in the general case. Since the magnetic moment $\boldsymbol{\mu}_{n\nu}$ should be real, this implies that to any vector $\boldsymbol{k}$ is associated the vector $-\boldsymbol{k}$ with

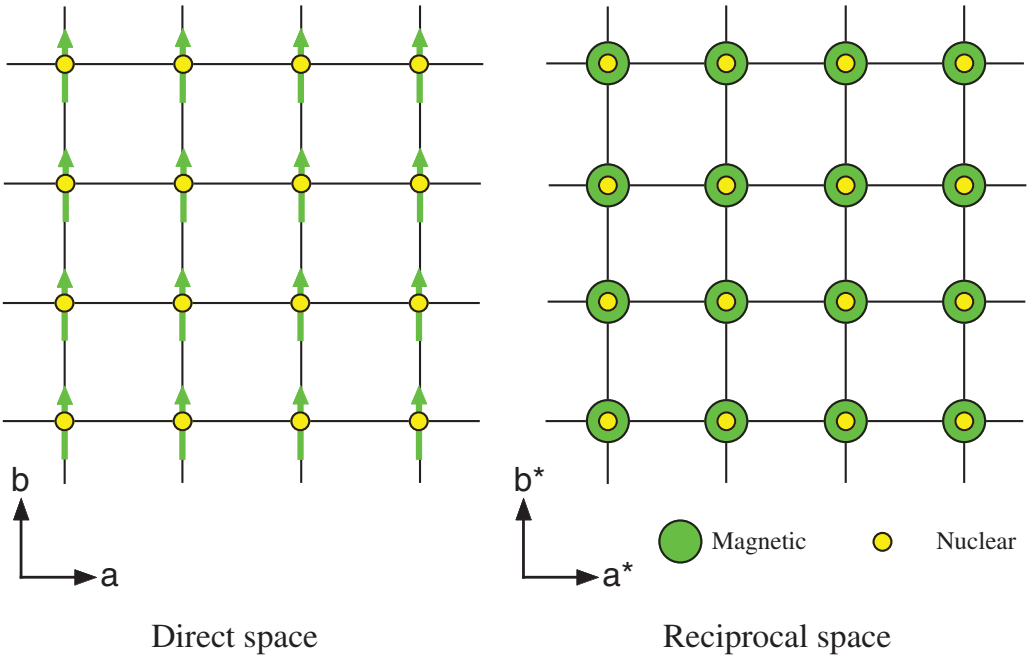

Figure 1. Ferromagnetic structure with $\boldsymbol{k} = (0, 0, 0)$.

$\boldsymbol{m}_{\nu,-\boldsymbol{k}} = (\boldsymbol{m}_{\nu,\boldsymbol{k}})^*$. This is true except for certain particular values of $\boldsymbol{k}$, such as $\boldsymbol{k} = 0$, or for some points on the surface of the Brillouin zone, for which $e^{-i\ \boldsymbol{k}\cdot\boldsymbol{R}_n}$ is always real. In these cases, only one vector $\boldsymbol{k}$ enter the summation.

3.2 Application: Classification of magnetic structures

From the precedent definition of the propagation vectors, it is now possible to classify the magnetic structures. This is done usually according to the number and the modulus of the vectors $\boldsymbol{k}$, which can be either rational (e.g. 0, 1/2, 1/5…), defining a **commensurate** structure, or irrational for an **incommensurate** one. When there is only one vector $\boldsymbol{k}$ (eventually associated to $-\boldsymbol{k}$) in the expansion Eq. (3.1), the structure is called **single-k**. When several distinct vectors $\boldsymbol{k}$ enter the summation, the structure is called **multi-k**.

(a) Commensurate magnetic structures

- **Case of a magnetic Bravais lattice: One magnetic atom per primitive unit cell**

This is the simplest case where it exists only **one magnetic atom** per elementary unit cell. A single propagation vector $\boldsymbol{k} = 0$ corresponds to a **ferromagnetic** structure (Fig. 1). In this case, the magnetic intensity appears on top of nuclear reflections.

A single propagation vector $\boldsymbol{k} = \boldsymbol{H}/2$, corresponding to a symmetry point of the Brillouin zone, yields an **antiferromagnetic** structure (Fig. 2). For each of the 14 Bravais lattices, only a few of such points exist and define a distinct type of antiferromagnet. These points are given in Table 1. In this case, the magnetic scattering occurs at points of reciprocal space where there is no nuclear signal. For these

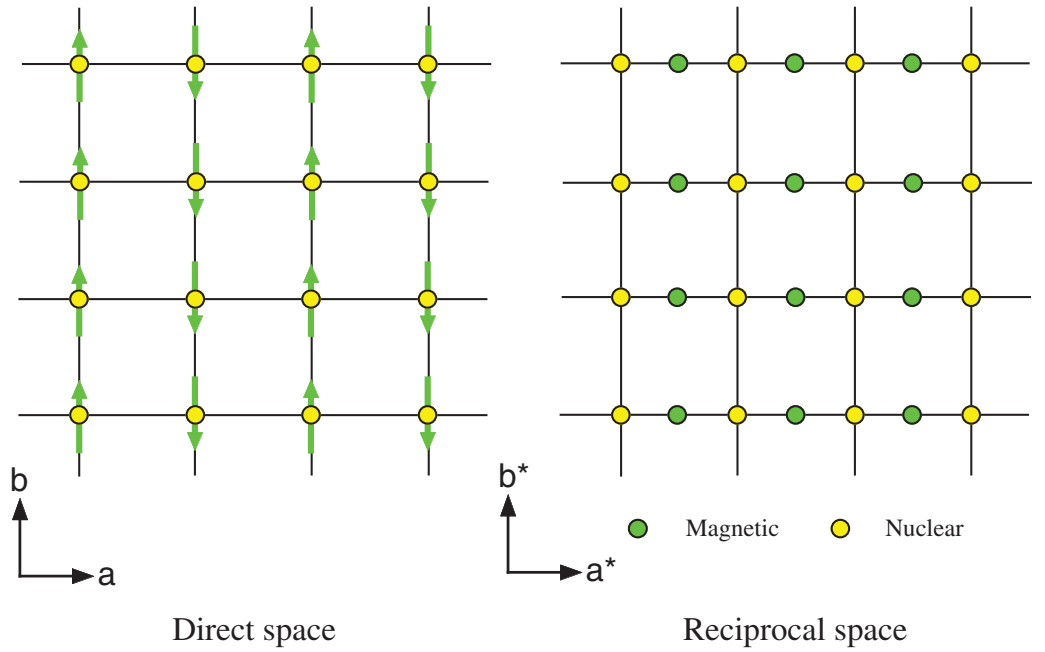

Figure 2. Antiferromagnetic structure with $\boldsymbol{k} = (\frac{1}{2}, 0, 0)$.

Table 1. Symmetry points $\boldsymbol{k} = \boldsymbol{H}/2$ of the Brillouin zone of the 14 Bravais lattices.

Cubic	P	$(0,0,\frac{1}{2})$	$(\frac{1}{2},\frac{1}{2},0)$	$(\frac{1}{2},\frac{1}{2},\frac{1}{2})$		
	I	$(0,0,1)$	$(\frac{1}{2},\frac{1}{2},0)$			
	F	$(0,0,1)$	$(\frac{1}{2},\frac{1}{2},\frac{1}{2})$			
Hexag.	P	$(0,0,\frac{1}{2})$	$(\frac{1}{2},0,0)$	$(\frac{1}{2},0,\frac{1}{2})$		
	R	$(0,0,\frac{1}{2})$	$(\frac{1}{2},\frac{1}{2},0)$	$(\frac{1}{2},\frac{1}{2},\frac{1}{2})$		
Tetrag.	P	$(0,0,\frac{1}{2})$	$(\frac{1}{2},0,0)$	$(\frac{1}{2},\frac{1}{2},0)$	$(\frac{1}{2},0,\frac{1}{2})$	$(\frac{1}{2},\frac{1}{2},\frac{1}{2})$
	I($c > a$)	$(0,0,1)$	$(\frac{1}{2},\frac{1}{2},0)$	$(\frac{1}{2},0,\frac{1}{2})$		
	I($c < a$)	$(1,0,0)$	$(\frac{1}{2},\frac{1}{2},0)$	$(\frac{1}{2},0,\frac{1}{2})$		
Ortho.	P	$(0,0,\frac{1}{2})$	$(\frac{1}{2},\frac{1}{2},0)$	$(\frac{1}{2},\frac{1}{2},\frac{1}{2})$		
	C($a > b$)	$(0,0,\frac{1}{2})$	$(1,0,0)$	$(\frac{1}{2},\frac{1}{2},0)$	$(1,0,\frac{1}{2})$	$(\frac{1}{2},\frac{1}{2},\frac{1}{2})$
	F($c > a > b$)	$(0,0,1)$	$(1,0,0)$	$(\frac{1}{2},\frac{1}{2},\frac{1}{2})$		
	I($c > a > b$)	$(0,0,1)$	$(\frac{1}{2},\frac{1}{2},0)$	$(\frac{1}{2},0,\frac{1}{2})$	$(0,\frac{1}{2},\frac{1}{2})$	
Monocl.	P	$(0,0,\frac{1}{2})$	$(0,\frac{1}{2},0)$	$(\frac{1}{2},0,\frac{1}{2})$	$(\frac{1}{2},\frac{1}{2},0)$	$(\frac{1}{2},\frac{1}{2},\frac{1}{2})$
	B($c > a$)	$(0,\frac{1}{2},0)$	$(0,0,1)$	$(\frac{1}{2},0,\frac{1}{2})$	$(0,\frac{1}{2},1)$	$(\frac{1}{2},\frac{1}{2},\frac{1}{2})$
Tricl.	P	$(0,0,\frac{1}{2})$				

two cases, and only in these two cases, the Fourier component $\boldsymbol{m}_{v,\boldsymbol{k}}$ can be identified to the real magnetic moment $\boldsymbol{\mu}_{nv}$.

When $\boldsymbol{k}$ is rational and corresponds to a long period commensurate structure (e.g. 1/5), the formalism is exactly the same than for incommensurate structures and will be treated in the next section.

When several non-collinear vectors $\boldsymbol{k}$ enter the summation Eq. (3.1), the structure is called **multi-k**. A very simple example of such a structure is the case of a **canted** arrangement (Fig. 3). This structure is described by two components, a ferromagnetic one appearing on top of nuclear peaks and

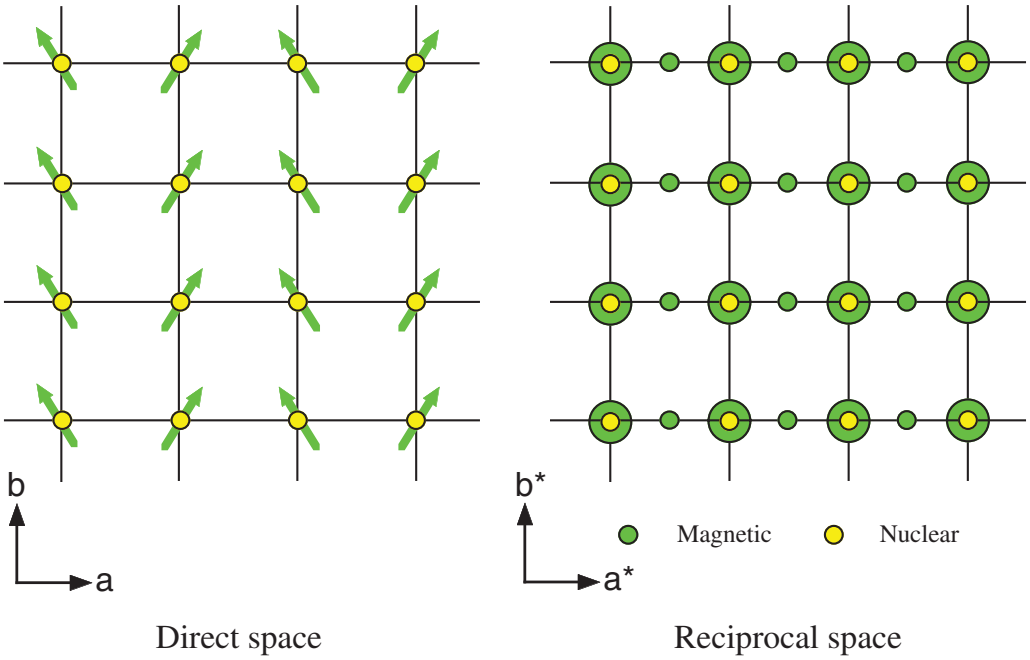

Figure 3. Canted structure with $\boldsymbol{k}_1 = (0, 0, 0)$ and $\boldsymbol{k}_2 = (\frac{1}{2}, 0, 0)$.

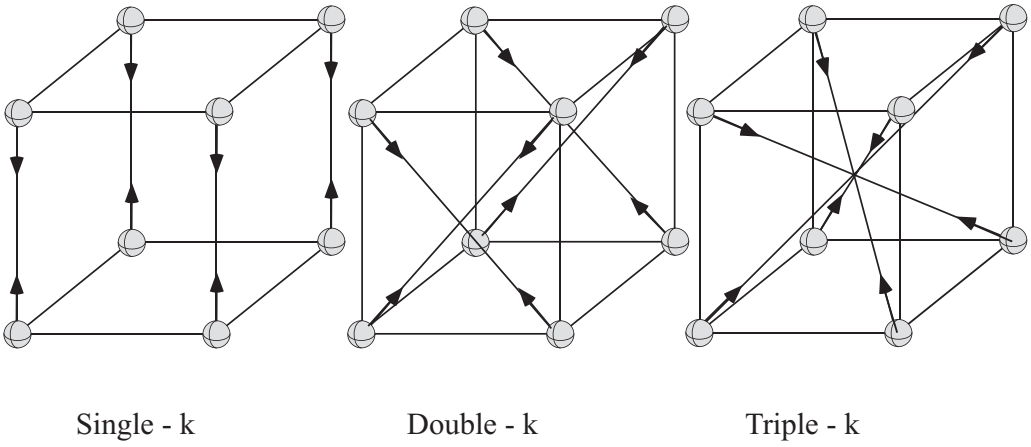

Figure 4. Multi-k structures associated to $\boldsymbol{k} = (0, 0, \frac{1}{2})$ in a primitive cubic lattice.

an antiferromagnetic one, which, in the case of a Bravais lattice, is purely magnetic and appears in a different place in reciprocal space.

In highly symmetrical compounds such as cubic space groups, much more complicated arrangements may occur. We will not describe them in details in this presentation. As an example, the single-k, double-k and triple-k magnetic structures with $\boldsymbol{m}_{\nu,\boldsymbol{k}} \parallel \boldsymbol{k}$ associated to the wave vector $\boldsymbol{k} = (0, 0, \frac{1}{2})$ in a primitive cubic lattice are depicted on Figure 4. The main difference between these structures is the orientation of the magnetic moments, which can be either along $\langle 100 \rangle$, $\langle 110 \rangle$ or $\langle 111 \rangle$. It

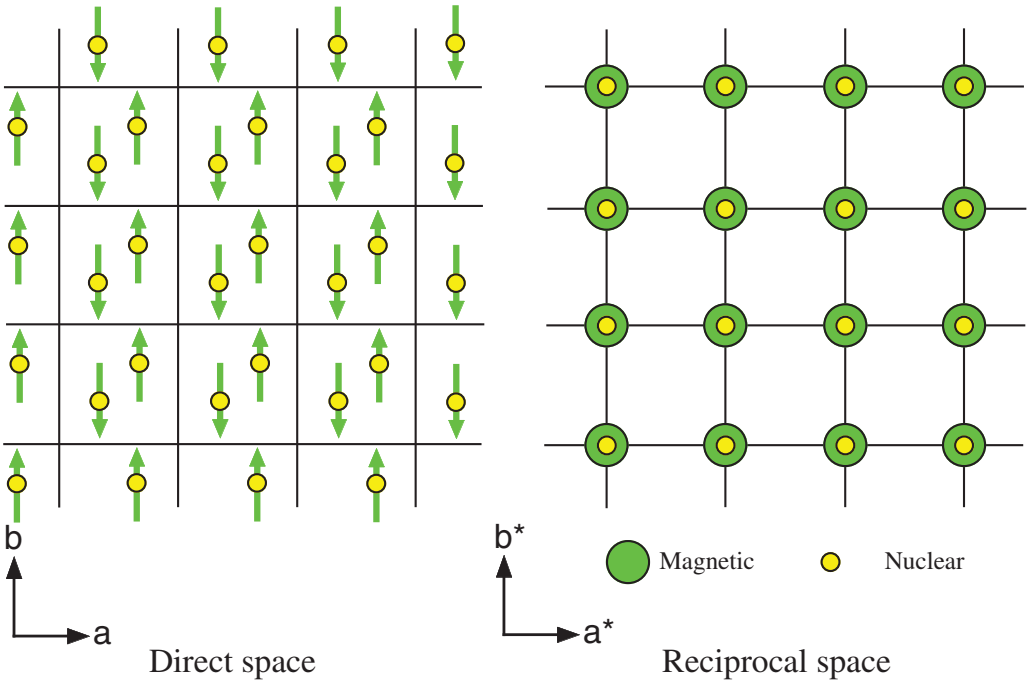

Figure 5. Antiferromagnetic structure with $\boldsymbol{k} = 0$ in the case of a non-Bravais lattice.

is often very difficult to distinguish between these three structures because of the existence of magnetic domains. One has to use an external constraint, such as an applied magnetic field along a particular axis or a pressure to validate one model or the other.

- **Non Bravais lattices: Several magnetic atoms per primitive unit cell**

When there are several magnetic atoms in the unit cell, the mutual orientations of their magnetic moments should be determined. It is important to realize that Eq. (3.1) tells us how a magnetic moment propagates from one unit cell to the other (translational symmetry) and not at all how the different Bravais lattices are coupled inside the unit cell. This scheme is given by the relative intensities of the magnetic peaks. Representation analysis can be of great help to reduce the number of independent parameters in the case of many Bravais sublattices. A complete presentation of the application of representation analysis to magnetic structures is a complex task out of the scope of this lecture. The reader interested in this aspect can consult references [4–6].

The main subtlety in the case of non-Bravais lattices arise from the fact that $\boldsymbol{k} = 0$ no longer implies a ferromagnetic structure. To illustrate this fact, let us consider a triclinic space group $P\bar{1}$ and an atom in a general position (xyz). The multiplicity of this site is two (xyz and $\bar{x}\bar{y}\bar{z}$). The antiferromagnetic structure drawn on Figure 5 corresponds to $\boldsymbol{k} = 0$, since atoms connected by translations of the lattice have the same magnetic moments. The magnetic scattering will thus appear at the same positions in reciprocal space than the nuclear one.

Depending on the space group, $\boldsymbol{k} = 0$ can correspond, in the case of non Bravais lattices, either to ferromagnetic structures, collinear antiferromagnetic ones, or even non collinear structures such as triangular ones. Only the intensities of the different magnetic peaks allow to distinguish between these different configurations.

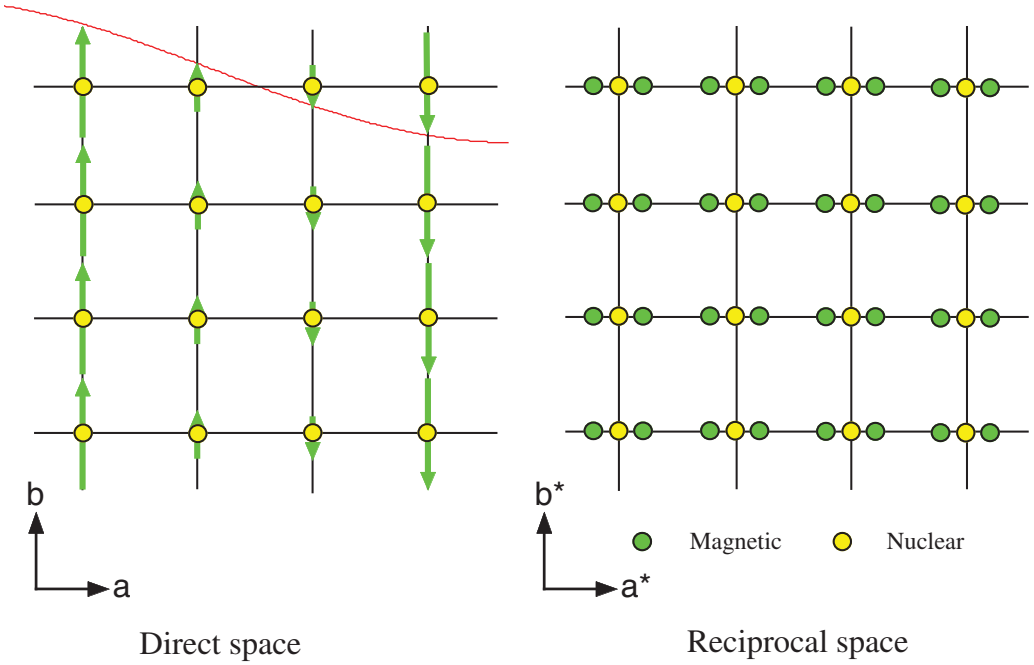

Figure 6. Sine-wave modulated structure with $\boldsymbol{k} = (k_x, 0, 0)$.

(b) Incommensurate magnetic structures

Let us consider now a magnetic ordering with $\boldsymbol{k}$ irrational. Two types of incommensurate structures should be defined: sine wave modulated structures and helical structures.

- **Sine-wave modulated structures**

The ordering is a sine-wave modulation of the moment value propagating along the $\boldsymbol{k}$ direction with an amplitude μ_v, a polarization along the vector $\hat{u}$ and a phase Φ_v (Fig. 6).

$$\boldsymbol{\mu}_{nv} = \mu_v \cdot \hat{u} \cos(\boldsymbol{k} \cdot \boldsymbol{R}_n + \Phi_v). \tag{3.4}$$

Such a moment distribution is described by two Fourier components, associated to $\boldsymbol{k}$ and $-\boldsymbol{k}$, namely $\boldsymbol{m}_{v,\boldsymbol{k}} = \frac{\mu_v}{2} \cdot \hat{u}\ e^{-i\Phi_v}$ and $\boldsymbol{m}_{v,-\boldsymbol{k}} = \frac{\mu_v}{2} \cdot \hat{u}\ e^{i\Phi_v}$. The two Fourier components are conjugated complexes. The magnetic structure factor becomes:

$$\boldsymbol{F}_M(\boldsymbol{Q} = \boldsymbol{H} + \boldsymbol{k}) = p \sum_v f_v(\boldsymbol{Q})\ \frac{\mu_v}{2} \cdot \hat{u}\ e^{-i\Phi_v}\ e^{i\,\boldsymbol{Q}\cdot\boldsymbol{r}_v}. \tag{3.5}$$

Many examples of such modulated structures have been found particularly in rare-earth and actinides compounds, and more recently in multiferroic systems. The polarization direction can be either longitudinal (collinear to the propagation) or transverse. If the modulus of $\boldsymbol{k}$ is irrational, all the moments inside the crystal have different moment amplitudes, whereas when this value is rational, the moments become the same after a period corresponding to the propagation. Since some of the magnetic moments cannot have their saturated value in such a sine-wave modulated structure, this kind of ordering is very often found close to the transition temperature, and does not persist on cooling down. At lower

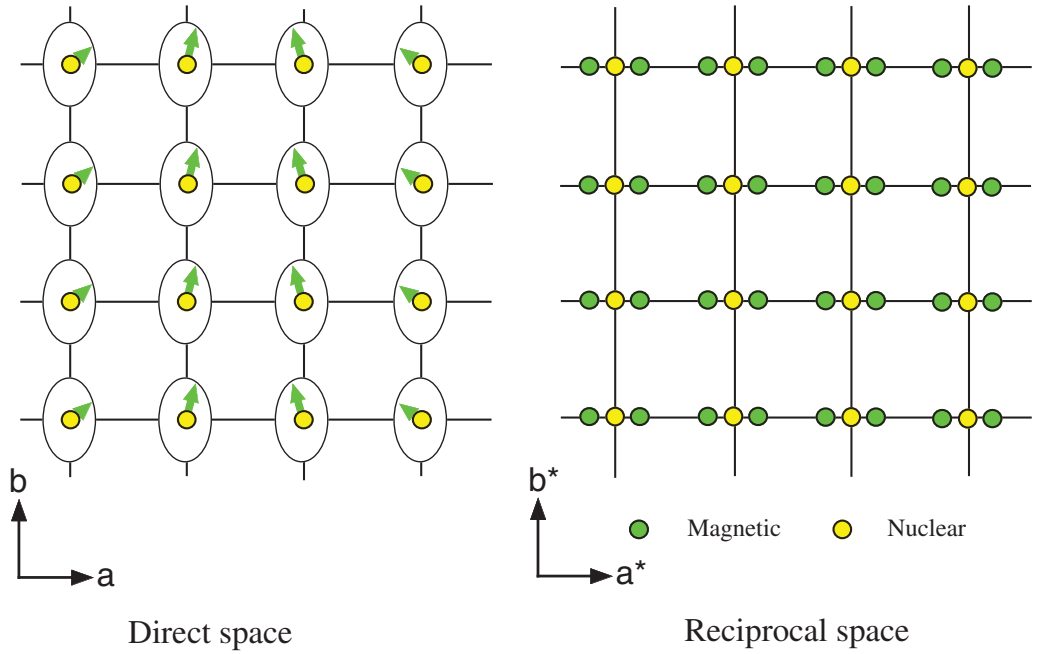

Figure 7. Helical structure with $\boldsymbol{k} = (k_x, 0, 0)$.

temperature, one often observes the apparition of harmonics (e.g. $\boldsymbol{k}/3$, $\boldsymbol{k}/5\ldots$) characteristics of a **squaring** of the structure, or a transition to a commensurate phase.

- **Helical structures**

In this kind of ordering, the magnetic moments rotate in a plane $(\hat{u}, \hat{v})$ when propagating along the $\boldsymbol{k}$ direction (Fig. 7) according to:

$$\boldsymbol{\mu}_{n\nu} = \mu_{1\nu} \cdot \hat{u}\ \cos(\boldsymbol{k} \cdot \boldsymbol{R}_n + \Phi_\nu) + \mu_{2\nu} \cdot \hat{v}\ \sin(\boldsymbol{k} \cdot \boldsymbol{R}_n + \Phi_\nu). \tag{3.6}$$

When $\mu_{1\nu} = \mu_{2\nu}$ the helix is circular, but examples of elliptic helixes $\mu_{1\nu} \neq \mu_{2\nu}$ can also be found. One should notice that the sine-wave modulated structures defined in the previous section are just particular cases of helical structures for which $\mu_{2\nu} = 0$. The distribution is described by two complex conjugate Fourier components $\boldsymbol{m}_{\nu,\boldsymbol{k}}$ and $\boldsymbol{m}_{\nu,-\boldsymbol{k}}$ associated to $\boldsymbol{k}$ and $-\boldsymbol{k}$:

$$\boldsymbol{m}_{\nu,\boldsymbol{k}} = [\frac{\mu_{1\nu} \cdot \hat{u}\ + i\ \mu_{2\nu} \cdot \hat{v}}{2}]\ e^{-i\Phi_\nu} \tag{3.7}$$

$$\boldsymbol{m}_{\nu,-\boldsymbol{k}} = [\frac{\mu_{1\nu} \cdot \hat{u}\ - i\ \mu_{2\nu} \cdot \hat{v}}{2}]\ e^{i\Phi_\nu} \tag{3.8}$$

and the magnetic structure factor can be written as:

$$\boldsymbol{F}_M(\boldsymbol{Q} = \boldsymbol{H} + \boldsymbol{k}) = p \sum_\nu f_\nu(\boldsymbol{Q}) \left[\frac{\mu_{1\nu} \cdot \hat{u}\ + j\ \mu_{2\nu} \cdot \hat{v}}{2}\right] e^{-i\Phi_\nu}\ e^{i\,\boldsymbol{Q}\cdot\boldsymbol{r}_\nu}. \tag{3.9}$$

Helical structures, as opposed to sine-wave modulated structures, can remain stable down to very low temperature because on each magnetic atom, the moment can reach its saturated value. The combination of an helical spiral and a ferromagnetic or an antiferromagnetic component can give rise to **conical**

structures in which magnetic moments rotate at the surface of a cone. Nowadays, the term cycloid is very often encountered in the literature, in particular when multiferroic systems are concerned. It is nothing but a particular type of helix, for which the propagation vector lies in the plane of rotation of the magnetic moments.

3.3 Warning: The phase convention of the Fourier components

In all what precede, we have defined the Fourier components of the distribution of the magnetic moments by $\boldsymbol{\mu}_{nv} = \sum_{\boldsymbol{k}} \boldsymbol{m}_{v,\boldsymbol{k}}\ e^{-i\ \boldsymbol{k}\cdot\boldsymbol{R}_n}$. This gave us a magnetic structure factor equal to $\boldsymbol{F}_M(\boldsymbol{Q} = \boldsymbol{H} + \boldsymbol{k}) = p\sum_v f_v(\boldsymbol{Q})\, \boldsymbol{m}_{v,\boldsymbol{k}} e^{i\,\boldsymbol{Q}\cdot\boldsymbol{r}_v}$, where the phase in the exponential is calculated from the true scattering vector $\boldsymbol{Q} = \boldsymbol{H} + \boldsymbol{k}$. It exists in the literature another convention, where the Fourier components are defined as:

$$\boldsymbol{\mu}_{nv} = \sum_{\boldsymbol{k}} (\boldsymbol{m}_{v,\boldsymbol{k}})'\ e^{-i\ \boldsymbol{k}\cdot\boldsymbol{R}_{nv}} \tag{3.10}$$

that is are calculated from $\boldsymbol{R}_{nv} = \boldsymbol{R}_n + \boldsymbol{r}_v$, the actual position of atom (n, v) in cell n and not from the origin $\boldsymbol{R}_n$ of this cell n. This convention leads to different Fourier components related to the first ones through:

$$(\boldsymbol{m}_{v,\boldsymbol{k}})' = \boldsymbol{m}_{v,\boldsymbol{k}}\ e^{i\ \boldsymbol{k}\cdot\boldsymbol{r}_v} \tag{3.11}$$

and to a different expression of the structure factor:

$$\boldsymbol{F}_M(\boldsymbol{Q} = \boldsymbol{H} + \boldsymbol{k}) = p\sum_v f_v(\boldsymbol{Q})\, (\boldsymbol{m}_{v,\boldsymbol{k}})' e^{i\ \boldsymbol{H}\cdot\boldsymbol{r}_v} \tag{3.12}$$

where the phase in the exponential is calculated from the nuclear scattering vector $\boldsymbol{H}$ and no longer from the true scattering vector $\boldsymbol{Q}$. These two approaches are mathematically the same and lead fortunately to the same results. The different programs of magnetic structure refinement use either one or the other convention. Problems generally appears when calculating the real magnetic moments carried by the different atoms from their Fourier components. A mixing of the two conventions is a classical trap which may lead, by adding wrong phase terms, to a completely wrong picture of the magnetic structure. Examples exist in the literature!

3.4 The phase problem of magnetic structures

We shall at this stage discuss an important limitation of the diffraction technique for determining **true magnetic structures**. The Fourier components of the distribution of the magnetic moments $\boldsymbol{m}_{v,\boldsymbol{k}}$ are complex vector defined with a phase factor Φ_v. For example, in the case of a sine-wave modulated structure, we have $\boldsymbol{m}_{v,\boldsymbol{k}} = \frac{\mu_v}{2} \cdot \hat{u}\ e^{-i\Phi_v}$. In a diffraction experiment, where the measurable quantity is proportional to the square of the modulus of the structure factor, the choice of an origin for this phase is arbitrary, since it corresponds only to a change of the origin of the whole crystal, and as a consequence this phase is lost. The only information that will give such an experiment is the phase difference between two different Bravais lattices in the case of a non-Bravais crystal.

Let us consider now a simple example of a Bravais lattice and a sine-wave modulated structure with $\boldsymbol{k} = 1/4$: when propagating along the $\boldsymbol{k}$ direction, we will have magnetic moments equal to $\boldsymbol{\mu}_{1v} = \mu_v \cdot \hat{u}\cos(\pi/2 + \Phi_v)$, $\boldsymbol{\mu}_{2v} = \mu_v \cdot \hat{u}\cos(\pi + \Phi_v)$, $\boldsymbol{\mu}_{3v} = \mu_v \cdot \hat{u}\cos(3\pi/2 + \Phi_v)$, $\boldsymbol{\mu}_{4v} = \mu_v \cdot \hat{u}\cos(2\pi + \Phi_v)\ldots$

The particular solution $\Phi_v = 0$ will give a $(0\ -\ 0+)$ sequence of the magnetic moments, that is two sites with no ordered moment and two sites with a maximum amplitude. If we now choose $\Phi_v = \pi/4$, the sequence becomes $(-\ -\ +\ +)$, that is a picture where all the atoms have the same constant moment. As far as the diffracted intensities are concerned, these two structures are indistinguishable. This is the

simplest case in which the physical picture depends on an arbitrary parameter not accessible by the experiment. Physical considerations are then required to prefer one model among others. For instance, a constant moment magnetic structure is normally expected at low temperature, and this argument may justify the choice $\Phi_\nu = \pi/4$ amongst all the others possibilities. Experimentally, other techniques may help to choose between several models. Unfortunately, there is no general method to overcome this difficulty.

4. EXPERIMENTAL TECHNIQUES

The expressions Eq. (3.2) and Eq. (3.3) of the differential magnetic cross sections and of the magnetic structure factors are the fundamental equations for a magnetic structure determination. In a measurement of coherent elastic scattering, the quantity actually determined is the **Bragg peak intensity**, that is the total number of neutrons entering the detector when passing through the Bragg condition of diffraction. This intensity corresponds to an integration of the differential cross-sections and is proportional to $|F_N(\boldsymbol{Q})|^2$ for the nuclear scattering and $|\boldsymbol{F}_{M\perp}(\boldsymbol{Q})|^2$ for the magnetic one, the coefficient of proportionality or scale factor being the same for a given scattering angle. Comparing the integrated intensity of a nuclear peak to the square of its nuclear structure factor gives immediately this scale factor, which can then be used to determine the amplitude of the magnetic moments from the magnetic peaks. In the case of a mixed reflection where both nuclear and magnetic signals appear, and for **unpolarised neutrons**, there is no interference effect and the intensity is simply proportional to the sum of these two quantities. In practice, a determination of a magnetic structure requires three steps: (i) the identification of the propagation vectors $\boldsymbol{k}$, (ii) the determination of the coupling between the Fourier components $\boldsymbol{m}_{\nu,\boldsymbol{k}}$ and (iii) the determination of the direction and amplitudes of these Fourier components, giving the direction and amplitudes of the true magnetic moments.

Magnetic structures can be investigated either on a powder specimen or a single crystal. Each technique has his own advantages and his own drawbacks, that we will discuss now.

4.1 Powder diffraction

When nothing is known, the best way to start is to use a powder specimen on a dedicated diffractometer. The sample is usually contained in a cylindrical sample holder illuminated by a monochromatic beam of neutrons. Such a sample consists of many small single crystals with random orientations over a 4π solid angle so that for each scattering vector a fraction of them fulfills the Bragg law. The diffraction diagram is recorded either by an array of detectors, or by a position sensitive detector (Fig. 8). This last kind of detectors has been a breakthrough in the technique because they have enormously increased the efficiency of such measurements [7]. They are constituted of up to 1600 cells of detection covering from 80° up to 160° angle. A full pattern is thus recorded in one shot, without having to move the detector. The measuring time is reduced compared to a single detector by a factor roughly equal to the number of detection cells. In addition, different pieces of equipment can be mounted around the sample to reach the necessary conditions of temperature, pressure or applied magnetic fields.

Another reason explaining the success of powder diffraction comes from the improvements in the way to analyze the data. The main problem encountered in powder diffraction arises from the so-called peak overlapping in the diagrams. Indeed, two reflections having nearly the same modulus of $\boldsymbol{Q}$ will enter the detector nearly at the same position. Depending on the experimental resolution, it is then very difficult, or impossible to know the relative intensities of these two lines to use them in a classical refinement based on integrated intensities. Only the sum of the two intensities is known.

The profile analysis method, or Rietveld method [8], has been another breakthrough for the technique. The positions and the intensities of the Bragg peaks for the whole scattering pattern are calculated from a parametrized model assuming a certain shape of the peaks and a width of these peaks

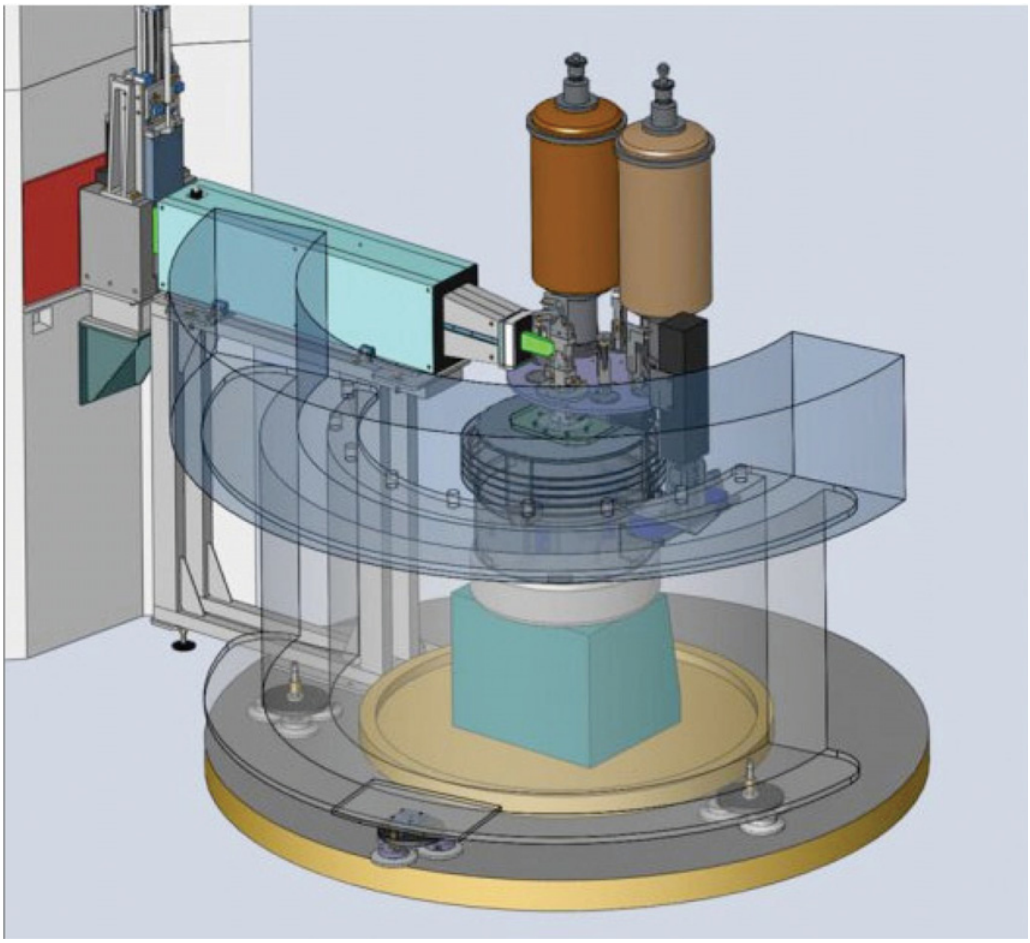

Figure 8. The powder diffractometer D2B at the Institut Laue Langevin.

varying according to the experimental resolution. The parameters of the model are least-squares fitted so that the calculated pattern reproduces the observed one, allowing to determine separately very close Bragg peaks. This method requires more computational effort than a classical least-squares refinement from integrated intensities, but today, with the power of modern computers, this is no longer a problem as it was in the past and this method can be applied to rather complicated structures. The program FULLPROF [9] is an example of software using this kind of approach that has been adapted to both nuclear and magnetic structure determinations (amongst many other possibilities).

The recorded intensities in such a measurement are both of nuclear and of magnetic origin in the magnetically ordered state, while they are almost purely nuclear in the paramagnetic one. A simple subtraction of the two patterns recorded on both sides of the transition temperature gives the pure magnetic signal, if no crystallographic transition occurs at the same time. This tells immediately the Bragg angles of the magnetic lines, and therefore the modulus of the scattering vectors where the magnetic signal appears. The problem is then to find one or several vectors $\boldsymbol{k}$ that could explain these values. This step can be the most difficult one of the structure determination. This search can be made by computer with several existing programs, or by hand with a graphical method [4]. It may happen that the measurement on a powder is not sufficient to determine unambiguously the propagation vectors.

The different hypothesis have then to be checked on a single crystal. Once the vector(s) $\boldsymbol{k}$ is (are) determined, the magnetic structure can be refined by testing the different possible coupling between the Fourier components $\boldsymbol{m}_{\nu,\boldsymbol{k}}$.

At this step, a severe limitation of the powder method should be explained. It is tightly connected to the previous problem of peak overlapping and concerns equivalent reflections. The integrated intensity measured on a powder diffractometer at one Bragg angle does not correspond to only one vector $\boldsymbol{Q}$, but to the superposition of all the equivalent vectors $\boldsymbol{Q}'$ deduced from $\boldsymbol{Q}$ by the symmetries of the crystal. As the magnetic structure is often less symmetrical than the crystal structure, those vectors $\boldsymbol{Q}'$ may be inequivalent as far as the magnetic structure is concerned. Since one measures only the sum of these contributions (same Bragg angle), a part of the information concerning the **direction** of the magnetic moments is lost. To illustrate this fact, let us consider a ferromagnetic structure. We have then:

$$\boldsymbol{F}_{M\perp}(\boldsymbol{Q}) = \sin\alpha\ \boldsymbol{F}_M(\boldsymbol{Q}) \tag{4.1}$$

where α is the angle between the moment direction and the scattering vector. The intensity in a powder sample is:

$$I_M(\boldsymbol{Q}) \propto p_M \langle \sin^2\alpha \rangle |\boldsymbol{F}_M(\boldsymbol{Q})|^2 \tag{4.2}$$

where p_M is the multiplicity of the peak and $\langle \sin^2\alpha \rangle$ is the mean value of $\sin^2\alpha$ over all the equivalent scattering vectors. As shown by Shirane [10], in the case of a cubic space group $\langle \sin^2\alpha \rangle$ is always equal to $2/3$ whatever the direction of the moment. This means that the moment direction cannot be determined in this case, the experiment will give only its amplitude. In the case of an uniaxial symetry (trigonal, tetragonal or hexagonal), the direction of the moment within the basal plane cannot be specified. For other symmetries, the moment direction can be determined without ambiguity. This rule has been illustrated here in the simple case of a ferromagnet, but the conclusions remain the same in all the other cases (antiferromagnetic, modulated structures . . .).

4.2 Single crystal diffraction

Two types of single crystal diffractometers exist. In the **4 circle geometry**, the crystal is mounted in an eulerian cradle (Fig. 9) so that any scattering vector can be placed in the horizontal plane by adjusting three angles ω, χ, ϕ. However, when the sample environment is complex (cryostats, furnaces, superconducting cryomagnets. . .), it is preferable to use a lifting counter diffractometer (Fig. 10), in which the only motion of the crystal is a rotation ω around the vertical axis. To measure Bragg intensities outside the equatorial plane, the counter can be lifted by an angle ν.

The previous section concerning powder diffraction may lead to think that experiments on single crystals bring more information than experiments on powder. This is true because in such experiments all the vectors $\boldsymbol{Q}$ can be investigated separately. The information does not loose its vectorial character and therefore we are no longer faced to the problem of an averaging over all the different $\boldsymbol{Q}$'s direction as it was the case with a powder experiment. However, we have to keep in mind that with real crystals life is not that simple, and that two main physical effects exist and bring some extra complications.

The first effect is the extinction. Without entering mathematical details, the main mani-festation of extinction is a weakening of strong reflections, resulting in intensities no longer proportional to the square of the structure factors as predicted by the kinematic theory. This is a major obstacle in getting accurate structure factors. Actually, the intensity diffracted by a crystal depends very much on its quality. For perfect crystals, the kinematic theory is no longer valid, and dynamical theory has to be used instead. In other cases, provided the effect is not too strong, corrections could be applied according to different models [11, 12], in which a real crystal is modeled by an assembly of perfect blocks of a certain size, with a misorientation described either by a Lorentzian or a Gaussian distribution. The size of the blocks and the width of the distribution are thus two parameters characteristics of a given crystal, and they could

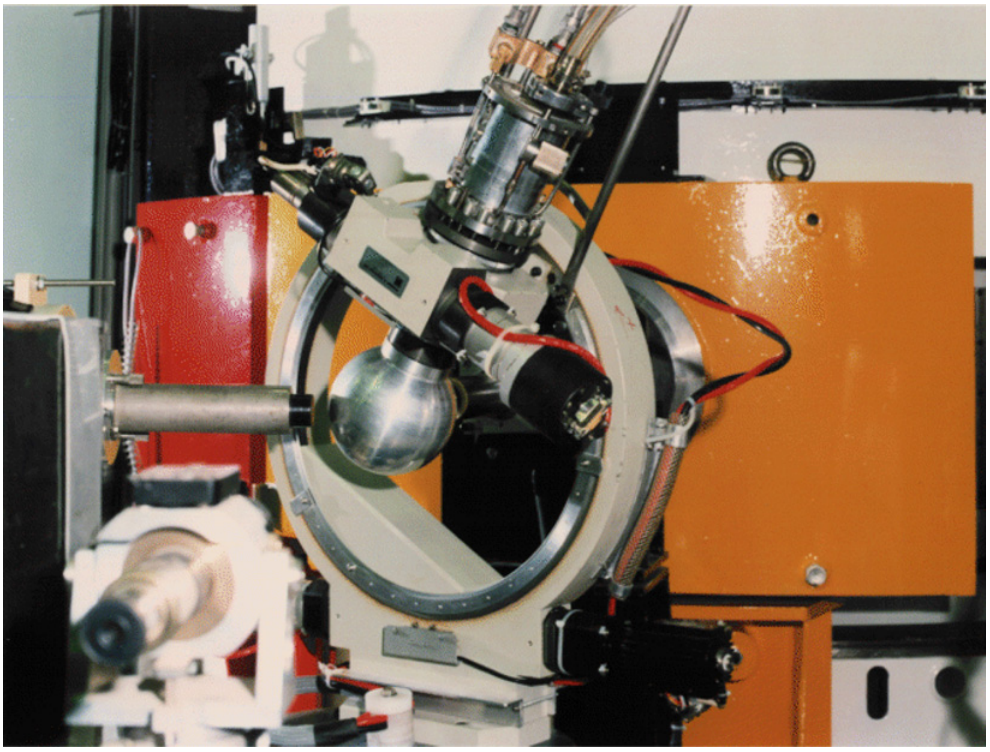

Figure 9. Close view of the Eulerian cradle with a displex cryo-refrigerator mounted on the 4 circle diffractometer D9 (Institut Laue Langevin).

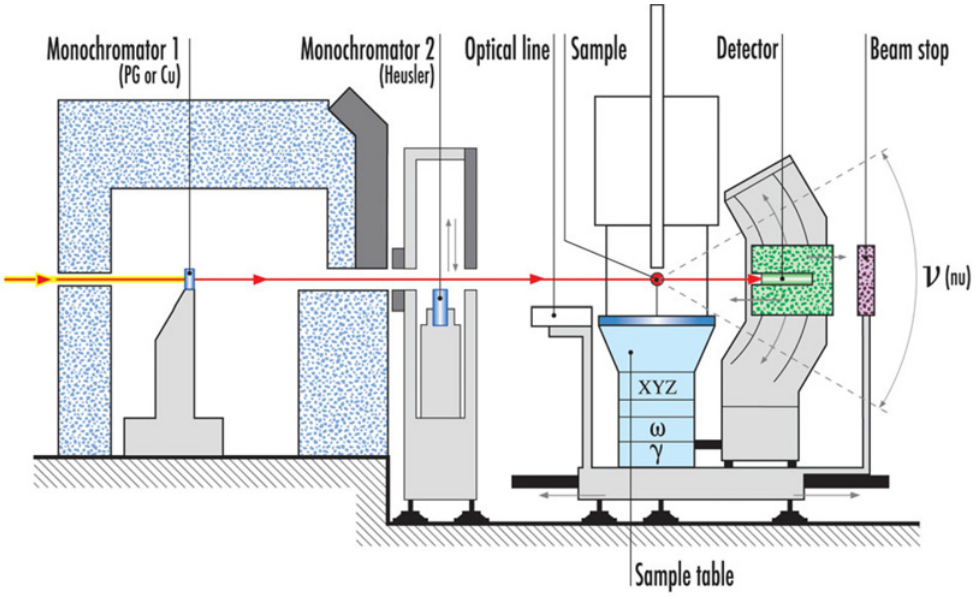

Figure 10. The lifting counter diffractometer D23 (Institut Laue Langevin).

The second limitation of single crystal measurements is connected to the so-called magnetic domains. For a given propagation vector $\boldsymbol{k}$, it exists several vectors $\boldsymbol{k}'$ derived from $\boldsymbol{k}$ by the symmetry operations of the crystallographic space group. This set of vectors $\boldsymbol{k}'$ is refered as the star of $\boldsymbol{k}$. When the ordering occurs, the crystal split into domains usually of the same volume, each one being characterized by one particular member of the star of $\boldsymbol{k}$. These domains are called K domains. In addition, it may also exist another type of domains (S domains) inside each K domain: these domains are constituted by the different equivalent directions for the alignment of the magnetic moments, equivalent for both the crystal symmetry and the propagation vector of this K domain. Domains are described more extensively in the lecture on Polarized Neutron Diffraction in this textbook. In a single crystal experiment, all the different K domains will give different sets of magnetic reflections, and each one of these reflections will imply an averaging over the S domains, giving rise to the same kind of averaging problems as for powder.

Moreover, it is also very difficult to distinguish between a single-k structure with different K domains and a single-domain multi-k structure. Only experiments on single crystals where an external perturbation (uniaxial stress or magnetic field) is applied to unbalance the domain repartition are able to remove the ambiguity. This problem is more important for highly symmetric lattices, such as face centered cubic lattices, because the star of $\boldsymbol{k}$ contains many elements.

5. ILLUSTRATION: EXAMPLE OF A MAGNETIC STRUCTURE DETERMINATION

As already stated, the expressions Eq. (3.2) and Eq. (3.3) of the differential magnetic cross sections and of the magnetic structure factors are the fundamental equations for a magnetic structure determination. Such a task requires three steps, which are (i) the identification of the propagation vectors $\boldsymbol{k}$, (ii) the determination of the coupling between the Fourier components $\boldsymbol{m}_{\nu,\boldsymbol{k}}$ and (iii) the determination of the direction and amplitudes of these Fourier components. To illustrate these different points, we will take a real example of an investigation in a molecular compound, the $Cr[C(CN)_3]_2$ complex [13].

This compound crystallizes in the orthorhombic space group $Pnma$. Each metal site is three-connected to its nearest neighbors by the $[C(CN)_3]^-$ anion leading to triangular arrays of spins. Susceptibility measurements have evidenced a strong antiferromagnetic coupling leading to a magnetic phase transition around 9 K. In order to characterize this transition, a powder neutron diffraction experiment has been carried out at the high flux reactor of the Institut Laue-Langevin (Grenoble), on the 400 cells diffractometer D1B. Two patterns were recorded respectively at 2 and 15 K, using a liquid helium cryostat. The wavelength $\lambda = 2.527$ Å was used and provided by a focusing pyrolitic graphite monochromator. The sample was enclosed in a cylindrical vanadium container 7 mm in diameter and 5 cm in height. Figure 11 shows the two patterns recorded at both temperatures and the difference between these two spectra.

When there is no crystallographic transition at the magnetic ordering, the difference between two spectra recorded below and above the transition temperature is purely magnetic. In our case, we can clearly observe in the difference four peaks at low Bragg angles, whereas the contributions at higher Q values are broader (because of the increase in the density of peaks at high Bragg angles these contributions are certainly the sum of several magnetic peaks) and weaker (because the magnetic form factor decreases when Q increases). The most important observation is that these peaks are located at 2θ values where there is no nuclear contribution. This fact is a proof of the existence of a non-zero propagation vector describing the magnetic ordering, that is an antiferromagnetic like structure (in the most general sense of the term antiferromagnetic), as expected from susceptibility measurements.

Before any attempt to refine the magnetic structure, the nuclear one should be known. This wasn't the case for $Cr[C(CN)_3]_2$ when the neutron experiment started and actually the structure has been

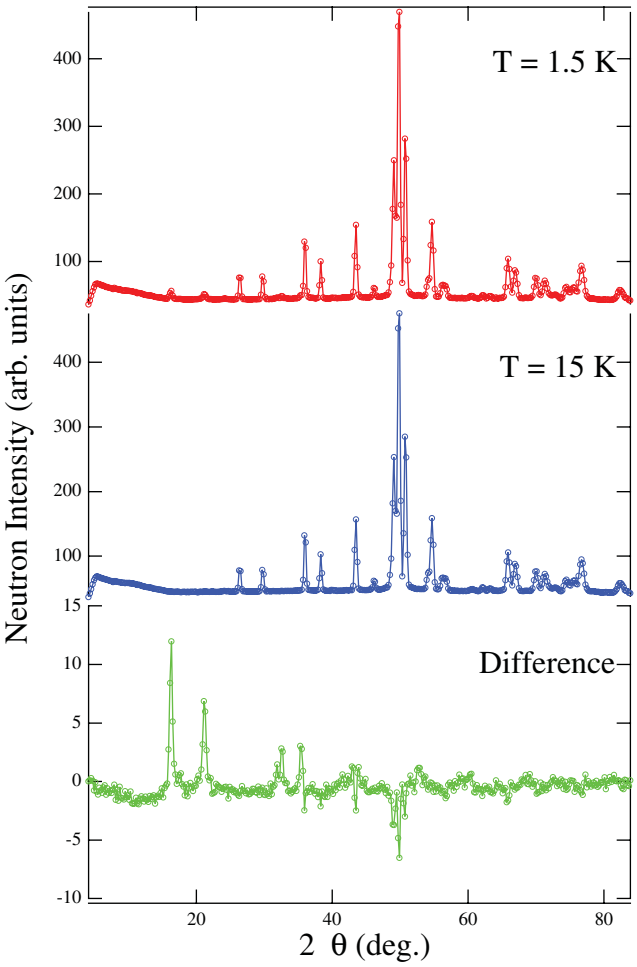

Figure 11. Powder diffraction patterns recorded below and above the transition temperature in the compound $Cr[C(CN)_3]_2$ and difference. From Ref. [13].

elucidated by Rietveld refinement of the powder neutron diffraction pattern recorded in the paramagnetic state ($T = 15$ K), using the software FULLPROF [9]. A gaussian function was chosen to generate the line shape of the diffraction peaks. The pattern is consistent with the crystal structure of the isotypic compound $Mn[C(CN)_3]_2$. All the reflexions can be indexed in the orthorhombic space group $Pmna$, the cell parameters being $a = 7.313(1)$ Å, $b = 5.453(1)$ Å and $c = 10.640(1)$ Å. The atomic positions have been refined starting from the values observed in the manganese derivative. Figure 12 shows the observed and calculated neutron diffraction profiles in the paramagnetic phase.

(a) Identification of the propagation vector

The usual procedure to identify the propagation vector is to start by determining the values of the Bragg angles of the magnetic peaks. The relation between these angles and the modulus of the corresponding

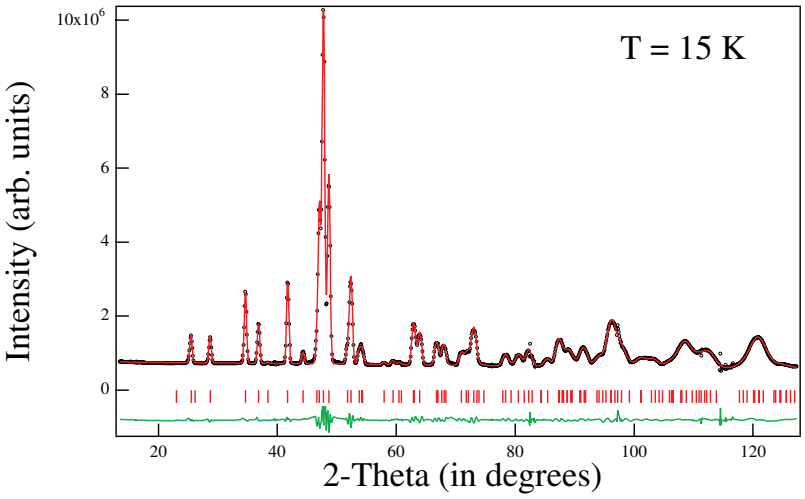

Figure 12. Observed and calculated powder neutron-diffraction patterns at T = 15K for the compound $Cr[C(CN)_3]_2$, as well as the difference (obs-calc). The ticks indicate the positions of the nuclear reflections. From Ref. [13].

scattering vectors $\boldsymbol{Q}$ is given by:

$$|\boldsymbol{Q} = \boldsymbol{H} + \boldsymbol{k}| = 4\pi \frac{\sin\theta}{\lambda} \cdot \tag{5.1}$$

The next step is then to find a vector $\boldsymbol{k}$ (or several) that could explain these values. The main difficulty in this step results from the vectorial nature of the relation $\boldsymbol{Q} = \boldsymbol{H} + \boldsymbol{k}$ when the powder experiment gives only the modulus of the vectors $\boldsymbol{Q}$.

To solve this problem, one could draw the reciprocal lattice associated to the crystallographic structure of the compound, together with the Brillouin zones of its Bravais lattice. By definition, each nuclear peak is then at the center of a Brillouin zone. The modulus of the magnetic scattering vectors previously determined allow to draw spheres centered **at the origin of the reciprocal lattice**. A very simple situation corresponds to the case where the lower angle magnetic peak belongs to the Brillouin zone of the origin of the reciprocal lattice. For this peak $\boldsymbol{H} = 0$ and $|\boldsymbol{Q}| = |\boldsymbol{k}|$. It is then possible to draw spheres of that radius **around each Brillouin zone center**. The intersections of these spheres with the previous ones define the possible wave vectors, as illustrated in the example of Fig. 13. Actually, since it is difficult to make a full drawing in 3D, the strategy usually employed consists to search within the main symmetry planes of the reciprocal lattice $((\boldsymbol{a}^*, \boldsymbol{b}^*), (\boldsymbol{a}^*, \boldsymbol{c}^*), (\boldsymbol{b}^*, \boldsymbol{c}^*)\ldots)$. Of course, for a completely general propagation vector, finding a solution this way may become very tedious. If there is no magnetic peak in the first Brillouin zone around $\boldsymbol{H} = 0$ (for instance if the magnetic moments are collinear to the propagation vector), the problem is even more complex. Several attempts should be made, starting from symmetry lines of the Brillouin zone. There is unfortunately no general recipe for such cases. However, it exists programs that generate propagation vectors within the first Brillouin zone in a systematic way, calculate from these propagation vectors the modulus of all the possible scattering vectors and compare these values with the observed ones. At the end, one could obtain a list of possible propagation vectors. Such programs make the job much easier. If none of these method works, the only way is then to make an experiment on a single crystal, and to make systematic scans within several Brillouin zones, trying to find where the magnetic signal is. This could also become a funny game!

In the particular case of $Cr[C(CN)_3]_2$, the propagation vector turned out to be $\boldsymbol{k} = (\frac{1}{2}, \frac{1}{2}, 0)$. This point is a particular symmetry point at the surface of the Brillouin zone describing an antiferromagnetic structure as stated in Table (1).

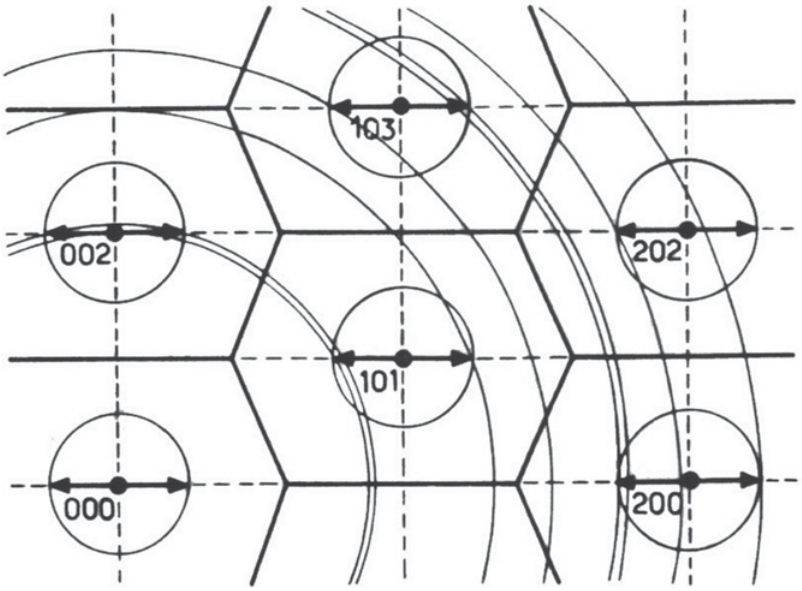

Figure 13. Graphic method to identify the propagation vector. From Ref. [4].

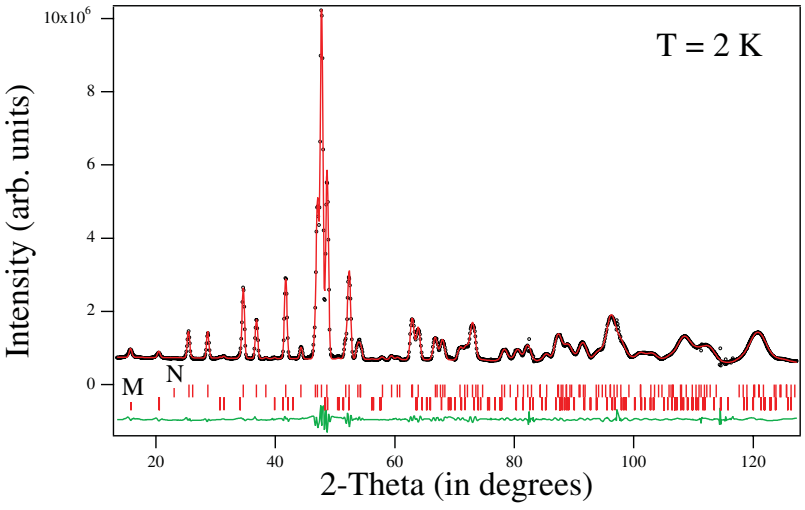

Figure 14. Observed and calculated powder neutron-diffraction patterns at T = 2K for $Cr[C(CN)_3]_2$, as well as the difference (obs-calc). The ticks indicate the positions of the reflections, for both the nuclear (N) and the magnetic (M) contributions. From Ref. [13].

(b) Coupling, direction and amplitudes of the Fourier components $m_{v,k}$

Once the propagation vector is determined, the next step consists in measuring magnetic integrated intensities. From these intensities and the knowledge of some nuclear peaks (to obtain a scale factor), one can deduce the modulus of $\boldsymbol{F}_{M\perp}(\boldsymbol{Q})$ for all the magnetic lines. From these values, it is then possible to determine the coupling, the direction and the amplitudes of the Fourier components $\boldsymbol{m}_{v,\boldsymbol{k}}$. Once again, this step does not give the true moment distribution, but its **Fourier decomposition**. When the structure

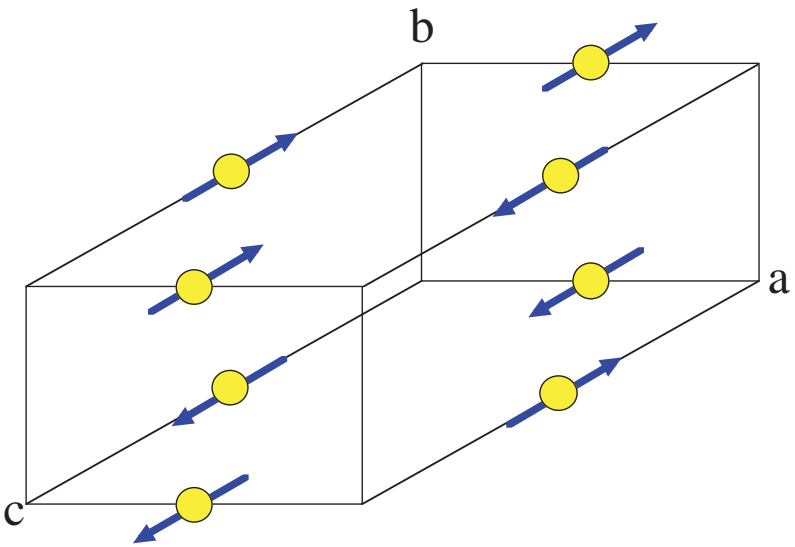

Figure 15. Schematic representation of the magnetic structure of $Cr[C(CN)_3]_2$ at 2K. For sake of clarity, only the Cr atoms of the unit cell have been represented. From Ref. [13].

is complex with many Bravais lattices, the number of possibilities to couple the Fourier components may be high. The representation analysis method is then useful to enumerate the possible couplings compatible with the symmetry of the compound. Moreover, the existence of systematic extinction rules for the magnetic signal should be tested since it can give indications concerning the moment direction. For instance the absence of any peak in the first Brillouin zone around $\boldsymbol{H} = 0$ in the case of a Bravais lattice tells immediately that moments are parallel to $\boldsymbol{k}$.

In $Cr[C(CN)_3]_2$, the Chromium atoms occupy a $(2b)$ site, with two Bravais lattices $(\frac{1}{2}, 0, 0)$ and $(0, 0, \frac{1}{2})$. Here the problem is very simple because the number of ways to couple the two sites is reduced. The best agreement (Fig. 14) is found for moments on the chromium atoms pointing along the c axis, in the sequence depicted on Figure 15.

This example of magnetic structure determination is an example for which powder diffraction was enough to completely solve the problem. In the chapter devoted to polarized neutron diffraction, other examples are given for which single crystal diffraction, even with polarized neutrons, was necessary to remove all the ambiguities.

6. CONCLUSION

The aim of these lecture notes was to remind both fundamental an practical aspects of magnetic structure determinations using neutron diffraction and to outline the unique information this technique can give. Due to the intensity of neutron beams of present sources an important constraint remains on the relatively large size of samples suitable for such experiments (compared to X-rays). However, the high potentiality and the uniqueness of this tool in solving solid state physics problems can justify all the efforts spent in growing such large samples.

Acknowledgements

I would like to thank V. Simonet and S. Petit for the extra opportunity offered with this chapter, and consequently for a critical reading of the manuscript during Christmas break!

References

[1] W. Marshall, S.W. Lovesey, *Theory of thermal neutron scattering*, Oxford Univ. Press (Clarendon), London and New York (1971).

[2] G.E. Bacon, *Neutron diffraction*, 3rd Ed. Oxford Univ. Press (Clarendon), London and New York (1975).

[3] G.L. Squires, *Thermal neutron scattering*, Cambridge Univ. Press, London and New York (1978).

[4] J. Rossat-Mignod, *Neutron Physics*, Chap. 20, Eds. Skold and Price, Academic Press (1987).

[5] J. Schweizer, *Neutron and Synchrotron radiation for condensed matter studies*, HERCULES, Vol. II, Chap. 5, Eds. Baruchel, Hodeau, Lehmann, Regnard, Schlenker, Les Editions de Physique, Springer-Verlag (1994).

[6] *Contribution of Symmetries in Condensed Matter*, Eds. B. Grenier, V. Simonet and H. Schober, EPJ Web of Conferences, EDP Sciences (2012).

[7] P. Convert, J.B. Forsyth, *Position sensitive detection of thermal neutrons*, Eds. Convert and Forsyth, Academic Press, New York (1983), 1.

[8] H.M. Rietveld, Acta. Cryst. **22** (1967), 151.

[9] J. Rodriguez-Carvajal, Physica B **192** (1993), 55.

[10] G. Shirane, Acta. Cryst. **12** (1959), 282.

[11] W.H. Zachariasen, Acta. Cryst. **23** (1967), 558.

[12] P. Becker, P. Coppens, Acta. Cryst. **A30** (1974), 129.

[13] J.L. Manson, E. Ressouche, J.S. Miller, Inorg. Chem. **39** (2000) 1135.